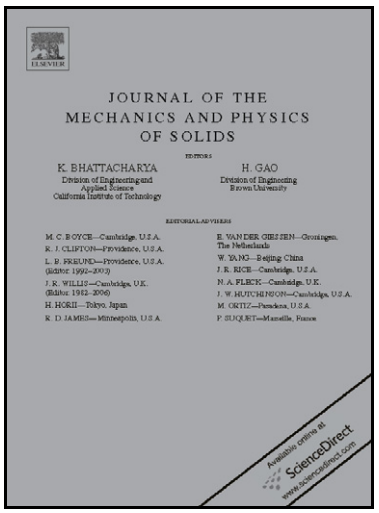

www.elsevier.com/locate/jmps

Grain misorientation and grain-boundary rotation dependent mechanical properties in polycrystalline graphene

Jiangtao Wu, Yujie Wei

PII: S0022-5096(13)00025-2
DOI: http://dx.doi.org/10.1016/j.jmps.2013.01.008
Reference: MPS2268

To appear in: *Journal of the Mechanics and Physics of Solids*

Received date: 26 June 2012
Revised date: 7 December 2012
Accepted date: 25 January 2013

Cite this article as: Jiangtao Wu and Yujie Wei, Grain misorientation and grain-boundary rotation dependent mechanical properties in polycrystalline graphene, *Journal of the Mechanics and Physics of Solids,* http://dx.doi.org/10.1016/j.jmps.2013.01.008

Grain misorientation and grain-boundary rotation dependent mechanical properties in polycrystalline graphene

Jiangtao Wu, Yujie Wei*

LNM, Institute of Mechanics, Chinese Academy of Sciences, Beijing 100190, China

Abstract: In two-dimensional polycrystalline graphene, two angular degrees of freedom (DOF) are needed to define a general grain boundary (GB): the misorientation of two grains and the rotation of the boundary line. Via both molecular dynamics simulations and theoretical analysis, we see that the density of GB defects strongly depends on grain misorientation but is insensitive to GB rotation. And reveal the dependence of mechanical properties on grain misorientation and GB rotation in polycrystalline graphene. We find that the dependence of GB normal strength on grain misorientation and GB rotation in graphene stems from the superposition of the stress field induced by a pentagon-heptagon pair itself to that from the interaction between the other defects and the one under consideration. Based on MD simulations and *ab initio* calculations, we show that failure starts from the bond shared by hexagon-heptagon rings. We then apply continuum mechanics to explain the dependence of GB normal strength on the two angular DOF in graphene with pentagon-heptagon rings. The investigation showed here supplies valuable guidance to develop multiscale and multiphysics models for graphene.

* To whom correspondence should be addressed: yujie_wei@lnm.imech.ac.cn

Keywords: polycrystalline graphene; pentagon-heptagon; grain misorientation; grain boundary rotation; disclination; molecular dynamics; density functional theory calculation

1. Introduction

The very recent and ongoing research in graphene has been extending, almost daily, the list of novel physical properties of graphene. Remarkable properties such as super electric conductance (Geim, 2009; Geim and Novoselov ,2007; Lin et al., 2010), high thermal conductance(Ghosh et al., 2008; Koh et al., 2010; Seol et al., 2010), and superb strength (Lee et al., 2008), etc., have been observed in graphene. The superb strength, combined with one or more specific aspects of other extraordinary properties, are currently considered to be promising in proposed technologies. For example, graphene is used as the reinforce component in composite materials, and is also considered as an ultrathin yet elastically stretchable membrane for electronic devices and for biological applications (Rogers et al., 2011, Kim et al., 2011). So far, the mechanical properties and deformation behaviour of pristine graphene or graphene with point defects have been intensively investigated (Ariza et al., 2010; Compton et al., 2012; Cranford et al, 2011; Koenig et al., 2011; Khare et al., 2007; Lee et al., 2008; Liu et al., 2007; Sen et al., 2010; Zhou and Huang, 2008; Zhang et al., 2006, Wei et al., 2012). Driven by the need for large-area graphene in engineering practice, polycrystalline graphene are broadly synthesized (Kim et al., 2009; Li et al., 2009; Reina et al., 2009; Yu et al., 2011; Zhao et al., 2010). The presence of GBs in such polycrystalline graphene naturally brings in the question how GBs in polycrystalline graphene influences their performance (An et al. 2011; Cockayne et al. 2011; Grantab et al. 2010; Huang et al. 2011; Kim et al., 2011; Malola et al., 2010; Rasool et al., 2011; Wang et al., 2011; Wu et al., 2012; Yazyev and Louie, 2010a, 2010b,Zhang et

al., 2012). It is a typical structure-property relationship which has been investigated for centuries in different materials.

In three-dimensional polycrystalline counterparts, it is well known that defects like dislocations (Devincre et al., 2008; Nix and Gao, 1998; Taylor, 1934) or grain boundaries (Gleiter, 1989; Hall, 1951; Petch, 1953;) in bulk crystals can strengthen materials. For two-dimensional polycrystalline graphene, some progress on how typical defects in symmetrical tilt GBs in graphene influence its mechanical properties has been achieved (Ariza et al., 2010; Ariza and Ortiz, 2010; Grantab et al., 2010; Wei et al., 2012; Zhang et al., 2006). However, how general GBs influence the mechanical properties of polycrystalline grapheme remains unknown. Geometrically, a general GB in three-dimensional polycrystalline materials is characterized by five degrees of freedom, three from the relative rotation of adjacent grains and two due to the angular degrees of the planar GB (Hull and Bacon, 2011). For two-dimensional polycrystalline graphene, only two rotational degrees of freedom are needed to define a general GB, the misorientation between two grains (θ) and the rotation of the boundary line itself (ψ), as demonstrated in Fig. 1. In what follows, we refer θ as grain misorientation and ψ as GB rotation. The focus here is to present a comprehensive investigation on how the two angular degrees of freedom (θ and ψ) influence GB normal strengths, GB energies, and GB failure.

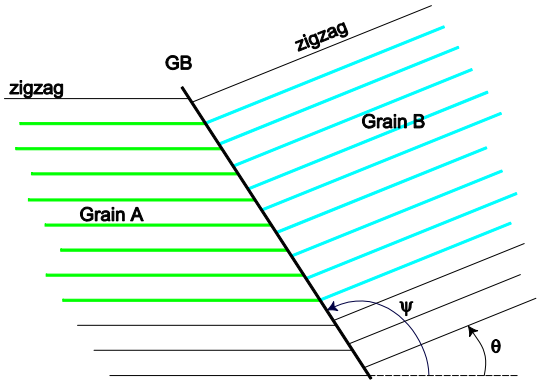

Fig. 1. Illustration for the two degrees of freedom in general GBs in graphene. GBs are characterized by two angular degrees of freedom – the misorientation between two grains (θ) and the rotation of the GB (ψ).

The work is organized as follows. We introduce the methods for all simulations in the next section. Detailed results for two groups of GBs are then presented. In section III, we study GBs with fixed GB rotation ψ but varied grain misorientation θ. Simulation results for fixed grain misorientation θ but varied grain rotation ψ are given in section IV. The failure mechanism of all samples is closely investigated in section V. We show that the disclination dipole model is capable to produce the stress fields induced by pentagon-heptagon rings. A conclusion is then made in section VI.

2. Numerical Methods

The Adaptive Intermolecular Reactive Empirical Bond Order (AIREBO) Potential (Stuart et al., 2000) for Carbon is used. Following Grantab et al. (2010), we have also used a switch function parameter r_{CC}=1.92Å (Table 1 in reference Stuard et al. (2000)), beyond which a carbon-carbon bond would break. Wei et al. (2012) have demonstrated that the stress-strain behaviour for pristine graphene from MD simulations by using the AIREBO potential with r_{CC}=1.92Å match well with those from first principle calculations. All simulations are performed at constant NVE integration in LAMMPS (Plimpton, 1995), and a simulated system has an initial temperature of 0K. It minimizes the strain rate effects in such quasi molecular static calculations. Still, limited by current computational resource, we only perform structure relaxation within a certain number of time-steps for each strain increment. So the strain rate effect remains. Our numerical tests show that the strain-strain responses become convergent as the applied strain rate is lower than 10^9 s^{-1}, which is the strain rate we applied in all simulations. A constant time step of 1 femtosecond is used. For a simulation box, periodic boundary condition (PBC) is applied along its

horizontal and vertical directions, and no constraint is applied to its thickness direction. In order to realize the PBC condition, a sample with two anti-symmetrical GBs is applied (see Fig. 2), with GBs perpendicular to the loading axis. Before loading, each sample is well relaxed to reach its energy minimum at almost zero pressure. After structure relaxation, uniaxial tension is then applied along the horizontal direction (perpendicular to the GBs) of the simulated box, whose typical dimensions are about 100nm in length and 30nm in width. Tension is applied by uniformly stretching the sample in horizontal direction but allow the box to shrink in the vertical direction (Plimpton, 1995). The atom stress was averaged over 500 time steps.

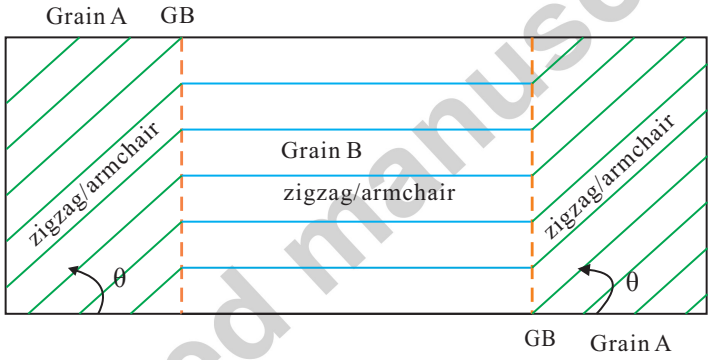

Fig. 2. Diagram of anti-symmetrical GBs to ensure periodic boundary conditions. The grain misorientation is either θ or π-θ.

The methods to construct symmetrical tilt GBs have been intensively documented. At the atomic level, tilt GBs in graphene are usually formed by typical defects of pentagon-heptagon rings (Ariza et al., 2010; Grantab et al., 2010; Hashimoto et al. 2004; Jeong et al. 2008; Liu et al., 2011; Meyer et al., 2008; Wei et al.,2012). In those tilt GBs, both grain misorientation θ (tilt angle) and GB rotation ψ change concurrently as tilt angles vary. Several groups have investigated the properties of tilt GBs (Grantab et al., 2010; Huang et al., 2011; Malola et al., 2010; Rasool et al., 2011; Yazyev and Louie, 2010a, 2010b; Wei et al.,2012). Here we focus on the dependence

of mechanical properties of general asymmetrical GBs on one variable (either θ or ψ) at a time.

To obtain asymmetrical GBs, we commonly use a trial and error method by gradually depositing atoms in the boundary of two patches of single crystalline graphene with prescribed grain misorientation θ and GB rotation ψ. Firstly, we cut two pieces of single crystalline graphene with prescribed grain misorientation θ and GB rotation ψ. We then insert and remove some atoms between the two single crystalline domains by introduce 5-7 rings and eliminate dangling bonds. At the end, we relax the whole structure. We iterate these steps until the GB structure reaches an energy minimum. The rationale behind the formation of the two prescribed angles stems from the way how polycrystalline graphene is synthesized by using chemical vapour deposition. Single crystalline graphene flakes grow from randomly distributed nucleation sites. As those flakes merge together, their rotational degree of freedom is constrained by the substrate. Flakes are then forced to stitch together at the initial misorientation θ and GB rotation ψ. Detailed atomic coordinates in GBs are determined by minimizing the energy in a simulation box where periodic boundary condition is applied. The obtained examples are then used for subsequent investigation. The GB energy is calculated as $\gamma=(E-NE_{pris})/2L_{GB}$, where E is the total energy of the structure with GBs, E_{pris} is the energy per atom of pristine graphene, N is the number of atoms, and L_{GB} is the length of the grain boundary.

3. Matched-zigzag and matched-armchair GBs: Fixed grain-boundary rotation

With the methods introduced above, we investigate the structural characteristics of GBs, and then explore the influence of grain misorientation to the mechanical properties of polycrystalline graphene. Now GB rotation ψ is a constant but we take grain misorientation θ as a variable. Two typical cases are considered here. We first put the zigzag direction as the edge of grain one, *i.e.*, $\psi=\pi/3$, and let this side merge

with the second grain to form a GB at a prescribed grain misorientation. In what follows, we name such type of GBs matched-zigzag GBs. Fig. 3a gives the atomic structures of several matched-zigzag GBs with different grain misorientations. We show, in turn, matched-zigzag GBs with misorientations of θ=4.7°, 10.9°, 14.7°, 19.1° and 27.5°, respectively. We see clearly that, in order to accommodate larger misorientation, higher density of pentagon-heptagon rings in the GB is required, so to minimize the GB energy. Similarly, we may put the armchair direction as one side of the GB in the first grain, and let the other grain with a certain misorientation adhere to the armchair boundary of the first grain, *i.e.*, $\psi=\pi/2$. Those GBs with $\psi=\pi/2$ are called as matched-armchair GBs. Detailed GB structures in matched-armchair GBs ($\psi=\pi/2$) are shown in Fig. 3b, where GB structures with grain misorientations of θ=6.6°, θ=14.7°, θ=19.1°, θ=23.4°, and θ=27.5°, are given.

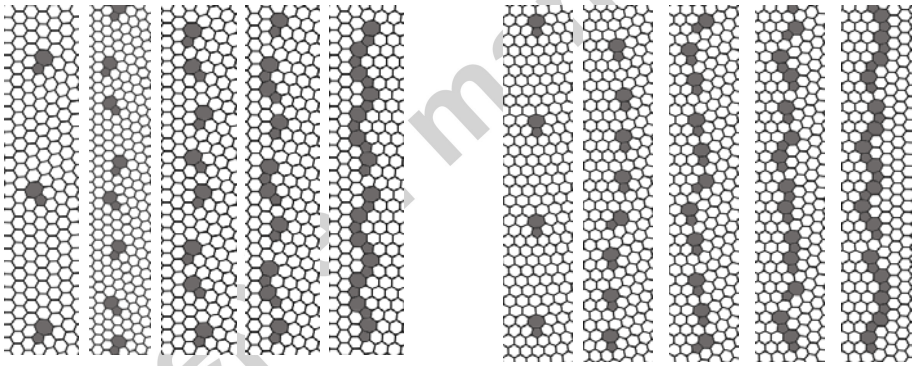

(a) (b)

Fig. 3. Atomic structures of matched-zigzag and matched-armchair GBs with constant GB rotation but varying grain misorientation. (a) Matched-zigzag GBs: the left grain is along zigzag direction, which corresponds to a constant GB rotation of $\psi=\pi/3$. The orientation of the right grain is chosen to give several different grain misorientations: θ=4.7°, 10.9°, 14.7°, 19.1°, and 27.5°, in turn. (b) Atomic structures of matched-armchair GBs. Here the boundary of the left grain is along armchair direction, which corresponds to $\psi=\pi/2$. The orientation of the right grain is chosen to give several different grain misorientations: θ=6.6°, 14.7°, 19.1°, 23.4°, and (e) θ=27.5°

The stress-strain curves obtained from MD simulations for those matched-armchair and matched-zigzag GBs are shown in Fig. 4a; curves for matched-zigzag GBs are given on the left side and those for matched-armchair GBs on the right side. For matched-zigzag GBs, GB normal strengths increase with grain misorientation increases. However, there is no clear correlation between GB strength and grain misorientation for matched-armchair GBs, as seen in Fig. 4b. GB energy as a function of grain misorientation is given in Fig. 4c. Unlike the apparent difference in strength as grain rotation changes, GB energy in those two types of GBs shows similar trends. We further explore the variation of initial stress in those GBs as a function of grain misorientation θ. Fig. 5a to 5c are, respectively, the contours of the normal stress component σ_{xx} for matched-zigzag GBs with θ=10.9°, 19.1°, and 27.5°. As a comparison, the stress contours of σ_{xx} for matched-armchair GBs with θ=14.7°, 19.1°, and 27.5° are shown in Figs. 5d to 5f, respectively. In matched-armchair GBs, we see clearly that the initial peak normal stress decreases with increasing grain misorientation. Given that the initial peak tensile stress reduces the strength of GBs, the variation of initial peaks stress with grain misorientation is consistent with the relationship for GB strength and grain misorientation obtained in Fig. 4b.

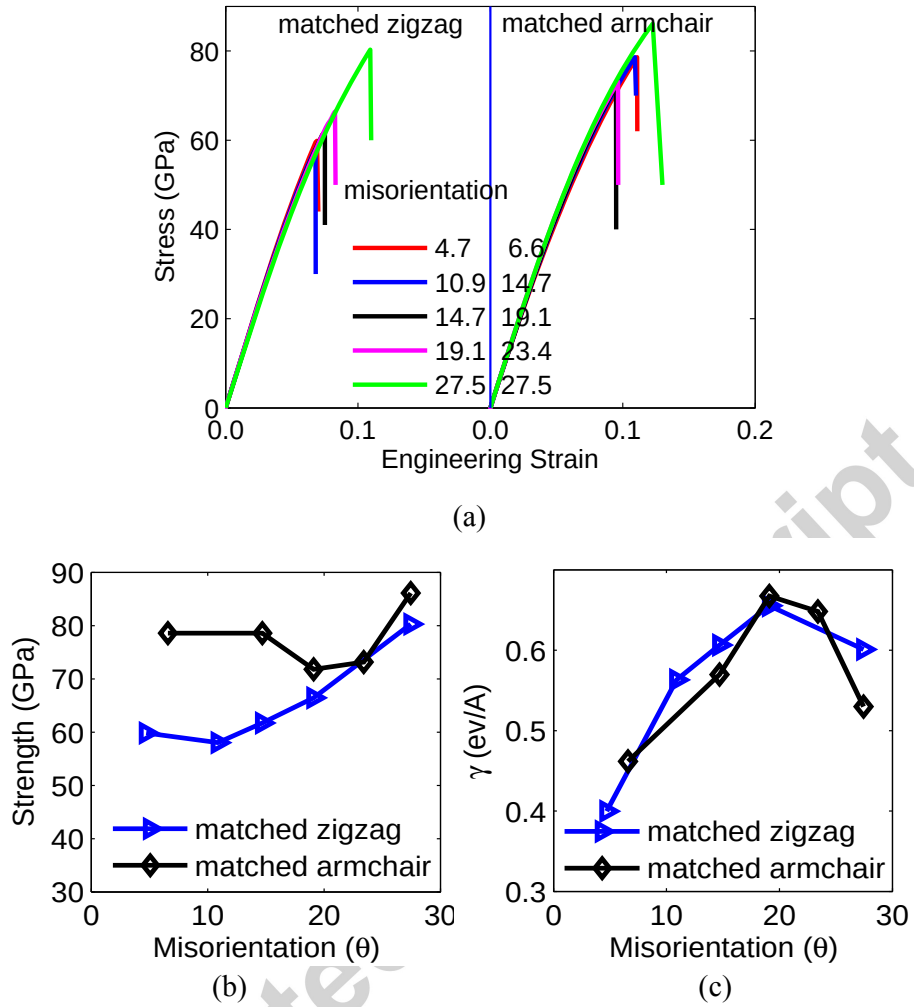

Fig. 4. Dependence of GB mechanical properties on grain misorientation. (a) Stress-strain behavior of matched-zigzag GBs (fixed GB rotation $\psi=\pi/3$, left) and matched-armchair GBs ($\psi=\pi/2$, right). (b) GB normal strength as a function of grain misorientation at constant GB rotation. (c) GB energy γ versus grain misorientation.

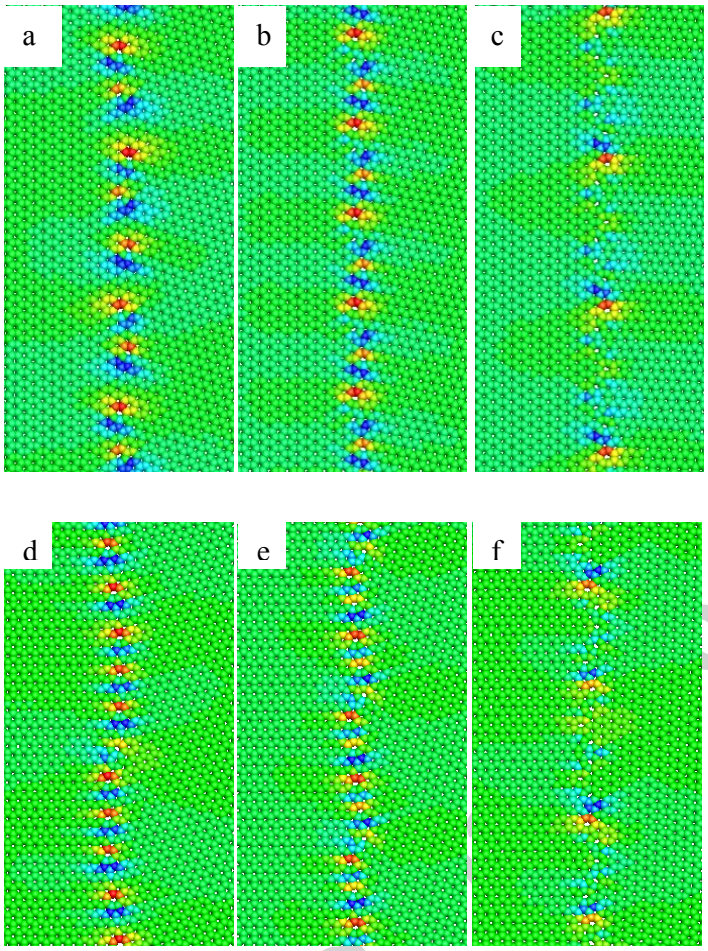

Fig. 5. Contours of stress component σ_{xx} with different grain misorientation θ but fixed GB rotation ψ. (a) to (c), Stress contours for matched-zigzag GBs ($\psi=\pi/3$): (a) $\theta=10.9^{o}$, (b) $\theta=19.1^{o}$, and (c) $\theta=27.5^{o}$. (d) to (f), Stress contours for matched-armchair GBs ($\psi=\pi/2$) : (d) $\theta=14.7^{o}$, (e) $\theta=19.1^{o}$, and (f) $\theta=27.5^{o}$. Peak positive stress is in red and peak negative in blue.

4. Mechanical behaviour in GBs with fixed grain misorientation

In the previous section, we investigate the mechanical properties of two types of GBs, where grain misorientation θ varies but GB rotation ψ is fixed. Here we explore the dependence of mechanical properties on ψ in polycrystalline graphene, i.e., θ is

now fixed but ψ is a variable. We start with the two matched-zigzag and armchair GBs with the same grain misorientation of θ=16.1. As demonstrated in Fig. 6, by rotating $\Delta\psi$ to the two GBs with initial rotation ψ_0=90^o, we yield a series of GBs with constant θ=16.1 but different ψ. Following the same procedures we introduced in Section 2, we generate corresponding GBs for matched-zigzag GB with several $\Delta\psi$, which are given in Fig. 7a. It is noted that defect density in GBs of different ψ is nearly the same, which suggests that defect density strongly depends on grain misorientation but not much on GB rotation. Figure 7b shows a series of atomic structures in GBs derived from the matched-armchair GB.

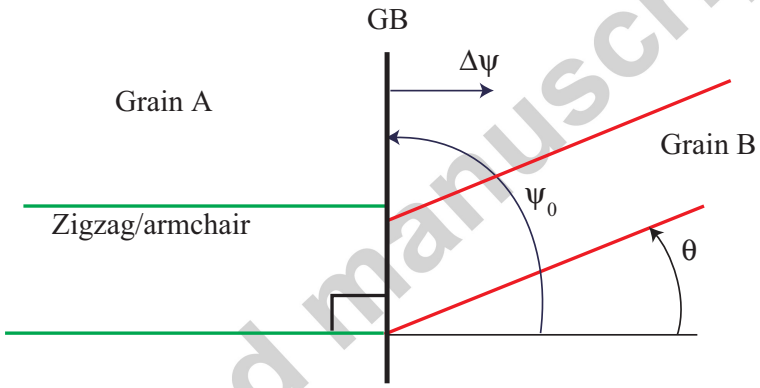

Fig. 6. Illustration of making GBs with a fixed grain misorientation of θ but varying the GB rotation ψ_0 by $\Delta\psi$. Recall that $\psi_0=\pi/3$ for matched-zigzag GBs and $\psi_0=\pi/2$ for matched-armchair GBs (the case shown here).

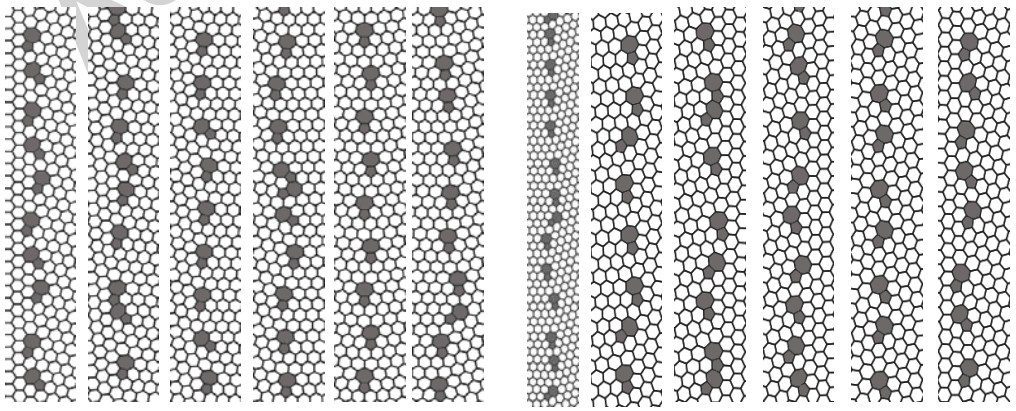

(a) (b)

Fig. 7. Atomic structures of derived GBs. (a) From the matched-zigzag GB with grain misorientation θ=16.1°. The change of GB rotation $\Delta\psi$ ranges from 0°, 6.6°, 10.9°, 16.1°, 22.4°, and 27.5°, as shown in turn. (b) GB structures in derived from the matched-armchair GB with grain misorientation θ=16.1, where GB rotation $\Delta\psi$ ranges from 0°, 6.6 °, 10.9 °, 16.1°, 22.4 °, and $\Delta\psi$=27.5 °, sequentially.

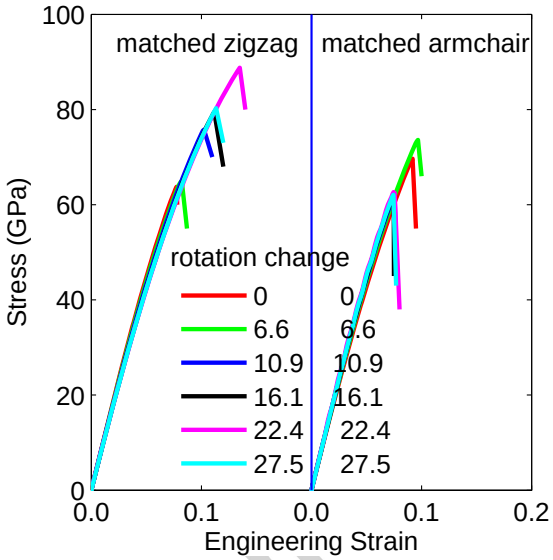

(a)

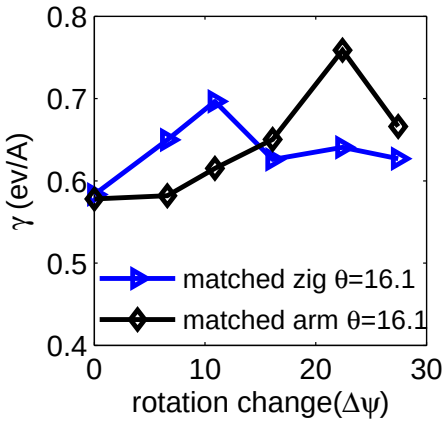

(b)

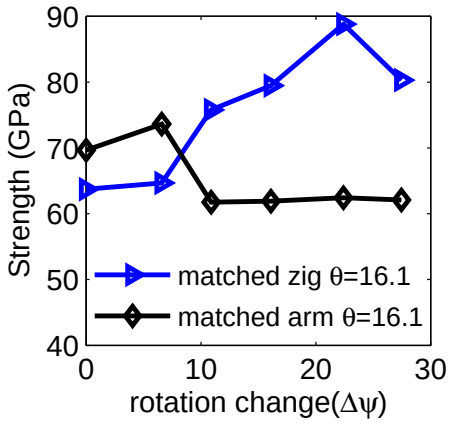

(c)

Fig. 8. The dependence of GB mechanical properties on $\Delta\psi$. (a) Stress-strain behavior of GBs with different rotation angles but constant grain misorientation; (b) GB normal strength as a function of GB rotation; (c) GB energy γ versus GB rotation.

In Fig. 8a, we show the stress-strain curves of the GBs given in Fig. 7. Curves on the left side in Fig. 8a are for GBs derived from the matched-zigzag GB with θ=16.1^o, and curves on the right side are for those GBs derived from the matched-armchair GB. GB normal strength as a function of GB rotation in Fig. 8b indicates that GB strength also depends on GB rotation. At the same grain misorientation θ=16.1^o, GBs derived from the matched-armchair GB show a slight weakening as GB rotation increases, while those from the matched-zigzag GB exhibit apparent strengthening as GB rotation increases. The change of GB energy with GB rotation is given in Fig. 8c.

5. GBs defects and the initial stress fields near GBs

Based on investigations shown in Section 3 and 4, we see that GB strength depends on both grain misorientation and GB rotation. Corollarily, we wonder what is the governing factor accounting for the observed results. Before addressing this question, we examine the process of GB failure. Snapshots given in Fig. 9 show the failure process in matched-zigzag GBs with grain misorientation θ=19.1^o. It is noted that bonds shared by hexagon-heptagon rings are subjected to the highest initial tensile stress (Fig. 9a). While straining, GB failure initiates from the bond shared by hexagon-heptagon rings (Fig. 9b). This bond failure is seen in other GBs, which is consistent with investigations for tilt GBs in graphene (Wei et al., 2012).

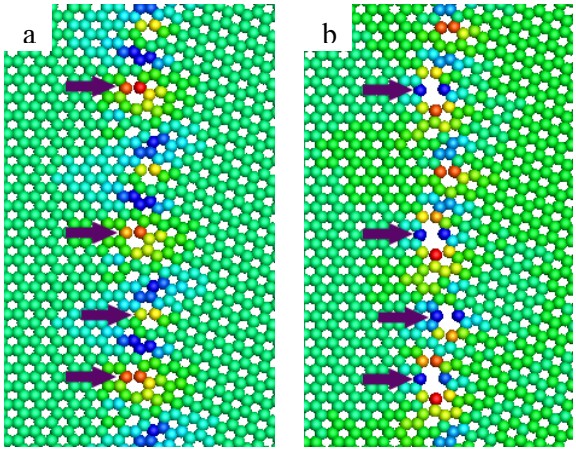

Fig. 9. The failure process in matched-zigzag GBs with grain misorientation θ=19.1^{o}. Contours show the stress field in the GB. (a) Initial stage, where bonds shared by hexagon-heptagon rings have the maximum tensile stress. (b) Failure initiates at the C-C bonds shared by hexagon-heptagon rings. Peak positive stress is in red and peak negative in blue.

The behind mechanism about why bond failure prefers to start at the hexagon-heptagon rings is further explored by using density functional theory (DFT) calculation. We perform the calculations with the Vienna Ab initio Simulation Package (VASP) code (Kresse and Furthmüller, 1996a, 1996b). The projector augmented wave (PAW) pseudopotentials (Blöchl, 1994; Kresse and Joubert, 1999) and the generalized gradient approximation (GGA) of the Perdew-Burke-Ernzerhof (PBE) functional (Perdew et al., 1996, 1997) are used. A plane-wave basis set with a kinetic-energy cut-off of 400 eV and a Monkhorst-Pack (Monkhorst, 1976) k-point mesh of 3×5×1 (Γ included) are used for static electronic structure calculations. Atoms are relaxed using a conjugate gradient algorithm until the interatomic forces

are less than 0.01eV/Å. A vacuum space of 20 Å along the direction perpendicular to the graphene sheets was used to eliminate the interactions between periodic images of graphene sheets. Periodic conditions are applied in the two in-plane directions by using the anti-symmetrical GB structures illustrated in Fig. 2. We choose two typical matched GBs, the matched-armchair GB with θ=6.6^{o} and the matched-zigzag GB with θ=19.1^{o} for DFT calculations. Figure 10a shows the electron density contour at the middle plane (z=0) for the whole sample with matched-armchair GBs. The dimensions of the simulation box are respectively 38.9 Å and 21.5 Å in x and y direction. It contains 316 atoms. Figure 10b highlights the pentagon-heptagon defect in the Fig. 10a. The amplified electron density contour for the defect is given in Fig. 10c. We clearly see that the electron density is the lowest in the two bond shared by the hexagon-heptagon rings. Figure 10d shows the electron density contour at the middle plane for the whole sample with matched-armchair GBs. For the defect composed of two pentagon-heptagon pairs highlighted in Fig. 10e. The electron density contour for the defect is given in Fig. 10f. We see that the electron density is the lowest (corresponding to the weakest bond) in the bond shared by the top hexagon-heptagon pair. These results from DFT calculations substantiate the findings from MD simulations (Wei et al., 2012).

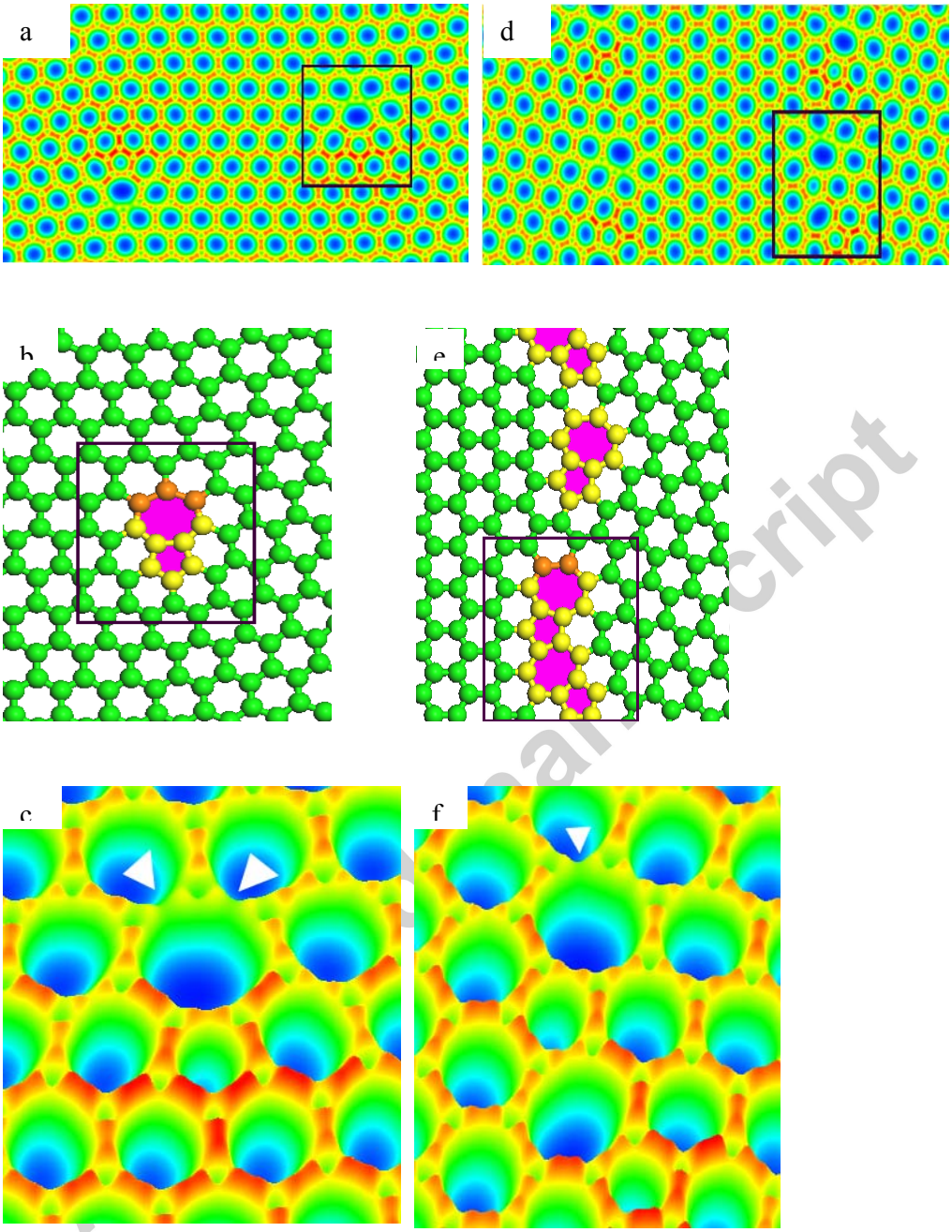

Fig. 10. The electron density contour at the middle plane (z=0, the grapheme lays in the x-y plane) to show the lowest electron density in the critical bond shared by hexagon-heptagon rings. The high peak of electron density is in red and zero electron density is in blue. (a) to (c), the matched-armchair GB with θ=6.6^{o}: (a) The electron density contour at the middle plane (z=0) for the whole sample; (b) Atomic view to highlight the pentagon-heptagon defect in (a); (c) Amplified electron density contour

for the boxed region in (b). (d) to (f), the matched-zigzag GB with θ=19.1^{o}. (d) The electron density contour for the whole sample; (e) The defect composed of two pentagon-heptagon pairs in sample (d); (f) The electron density contour for the boxed region in (e). Atoms forming the weakest bonds are colored differently in (b) and (e), and the locations of lowest electron density are pointed by white arrows.

Via both MD simulations and DFT calculations, we see that the critical points for failure initiation locate at the bond shared by hexagon-heptagon rings, and the GB strength is essentially determined by stress status at those points. We perform mechanical analysis to examine the initial stress at those critical points, in hope to reveal the correlation between GB normal strength and the two DOFs of a GB. We apply the disclination model to analyze the initial stress induced by hexagon-heptagon rings. The disclination model (Eshelby, 1966; Kleman and Friedel, 2008; Li, 1972; Muskhelishvili, 1953; Shih and Li, 1975; Romanov and Kolesnikova, 2009) has been successfully applied to explain the strength – tilt angle relation for tilted GBs (Wei et al. 2012) in graphene, as well as the boundary structures in silicon, germanium (Mullner and Pirouz, 1997), biomaterials (Yu and Sanday, 1991) and fullerenes (Kolesnikova and Romanov, 1998). Following Li (1972) and Wei et al. (2012), we consider a pentagon ring in the hexagonal graphene as a positive wedge disclination, and a heptagonal ring as a negative disclination. One pentagon-heptagon pair forms a disclination dipole. As seen in Figs. 3 and 7, a GB in graphene is composed of a series of disclination dipoles. Analogy to dislocations, disclination dipoles interact with other dipoles and may migrate as well under thermal or mechanical undulations (Warner et al. 2012; Kurasch et al., 2012). The local stress at the bond shared by

hexagon-heptagon rings is a superposition of the stress field induced by the disclination dipole under consideration and the stress fields by all other disclination dipoles.

The elastic fields of a straight disclination were given in literature (Eshelby, 1966; Huang and Mura, 1970; Li, 1972). Here we are interested in the stress fields by one disclination dipole shown in Fig. 13i. In the Cartesian coordinate, the stress components produced by the disclination dipole seen in Fig. 11a are (Eshelby, 1966; Huang and Mura, 1970; Li, 1972):

$$\sigma_{xx}(x,y,x_1,y_1,x_2,y_2) = D\omega\left[\ln\frac{r_1}{r_2} + \frac{(y-y_1)^2}{r_1^2} - \frac{(y-y_2)^2}{r_2^2}\right] \tag{1a}$$

$$\sigma_{yy}(x,y,x_1,y_1,x_2,y_2) = D\omega\left[\ln\frac{r_1}{r_2} + \frac{(x-x_1)^2}{r_1^2} - \frac{(x-x_2)^2}{r_2^2}\right] \tag{1b}$$

$$\sigma_{xy}(x,y,x_1,y_1,x_2,y_2) = -D\omega\left[\frac{(x-x_1)(y-y_1)}{r_1^2} - \frac{(x-x_2)(y-y_2)}{r_2^2}\right] \tag{1c}$$

where $D=G/[2\pi(1-\upsilon)]$ for plane strain condition and $D=E/4\pi$ for plane stress condition, (Muskhelishvili, 1953) ω is the strength of the disclination, $r_1^2=(x-x_1)^2+(y-y_1)^2$, and $r_2^2=(x-x_2)^2+(y-y_2)^2$. For a grain boundary composed of disclination dipoles, if the GB is constructed by an array of disclination dipole cluster evenly spaced by a periodicity L and there are m dipoles in each cluster, the total stress at (x, y) can be expressed as

$$\sigma = \sum_{k=-\infty}^{+\infty}\sum_{n=1}^{m}\sigma(x,y,x_{n1},y_{n1}+kL,x_{n2},y_{n2}+kL) \tag{2}$$

where (x_{n1}, y_{n1}), (x_{n2}, y_{n2}) are the locations of the n-th positive and negative disclinations, respectively. It is noted that t eqs. (1) and (2) are only applicable for flat graphene. In our calculations, graphene is subjected high level in-plane tension, which can suppress possible rippling in the graphene and make it flat.

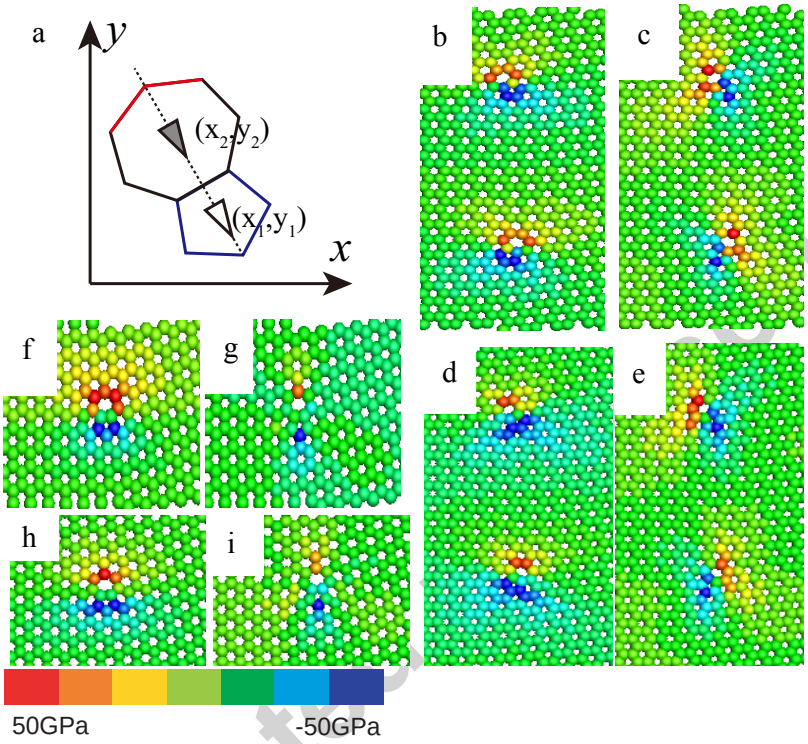

Fig. 11. Stress contours for GBs with different misorientation and a pentagon-heptagon pair forming a disclination dipole. (a) The Cartesian coordinates for a pentagon-heptagon pair forming a disclination dipole. Here (x_1, y_1), (x_2, y_2) are the locations of the positive and negative disclinations, respectively. (b), (c) stress components σ_{xx}, σ_{yy} by continuum mechanics using eq. (2) for matched-zigzag GB (θ =4.7^o); (d), (e) Corresponding results from MD simulations. (f), (g) Continuum mechanics results for matched-armchair GB (θ =6.6^o). (h), (i) Corresponding MD simulations.

Using equation (2), we calculate the stress fields induced by disclination dipoles in GBs. The stress contours from both continuum mechanics theory and based on MD simulations are shown in Fig. 11. Figure 11b and 11c show respectively the calculated contour of σ_{xx}, σ_{yy} for the matched-zigzag GB with θ=4.7°. As a comparison, the corresponding stress components from our MD simulations are shown in Fig. 11d and 11e, respectively. We see that the theoretical results based on disclination model capture well the stress patterns obtained from MD simulations. In addition, we find that the peak tensile stress occurs at the C-C bond shared by hexagon-heptagon rings, which is consistent with the failure process shown in Fig. 9. Fig. 11f and 11g show respectively the contours of σ_{xx}, σ_{yy} for the matched-armchair GB with θ=6.6°, and corresponding results from MD simulations are given in Fig. 11h and 11i.

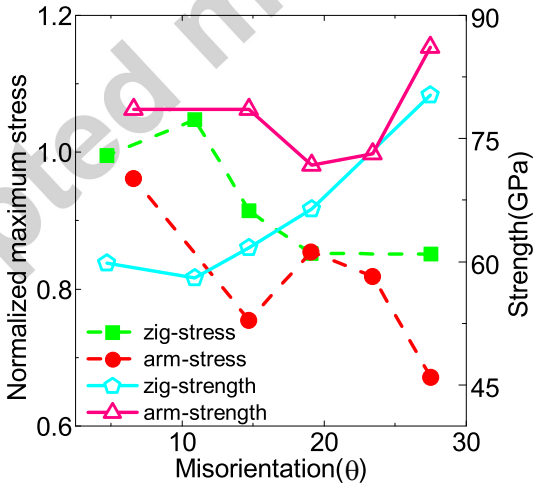

Fig. 12. Correlation between the maximum normal stresses in matched-zigzag (zig-stress) and matched-armchair (arm-stress) GBs and their respective GB strengths. The increase (decrease) in the maximum stress in the critical bond as a function of misorientation corresponds to the decrease (increase) in strength.

Since we know that bonding breaking initiates at the C-C bond between the hexagon and the heptagon rings from MD simulations, we then calculate the initial stresses along the breaking bond's direction by using the disclination model. The maximum stress along the C-C bond shared by hexagon-heptagon rings for samples with different grain misorientation is shown in Fig. 12. Since the larger the initial tensile stress is, the lower the strength will be. The variation of the maximum tensile stress in the critical C-C bond obtained by using equation (2) matches well with the GB strength from MD simulations, in the sense that the increase (decrease) in the tensile stress corresponds to the decrease (increase) in GB strength.

6. Conclusions

In summary, we use two degrees of freedom to characterize a general GB in polycrystalline graphene: the misorientation of two adjacent grains (θ) and the rotation of the boundary line (ψ). We investigate the dependence of mechanical properties on grain misorientation and GB rotation angle from two aspects: (a) matched GBs with fixed GB rotation (either along armchair or zigzag direction) and grain misorientation as a variable, and (b) GBs with fixed grain misorientation θ but GB rotation ψ changes. Simulations on GBs with fixed grain misorientation but different GB rotations suggest that, in addition to the misorientation, GB rotation also plays a significant role for the physical properties of GBs. The density of GB defects strongly depends on grain misorientation but is insensitive to GB rotation. Both our MD simulations and DFT calculations confirm that failure occurs in GBs, and

initiates from the bond shared by hexagon-heptagon rings but not the bond shared by pentagon-heptagon rings.

By applying the disclination dipoles in GBs, we show that there is a strong correlation between the variations of the maximum tensile stress along the critical C-C bond obtained by continuum mechanics with the GB strength obtained from MD simulations: the increase (decrease) in the tensile stress leads to the decrease (increase) in GB strength. This observation indicates that the initial stress induced by disclination dipoles controls the strength of GBs composed of pentagon-heptagon rings. Given that the electronic, optical, and phonon properties could be sensitive to mechanical properties in graphene (Castro et al., 2009; Pereira et al., 2009), this work supplies guidance for further development of multiscale and multiphysics models for graphene and other two dimensional structures.

Acknowledgements

The work is supported by the Chinese Academy of Sciences (CAS) via the Hundred Talent Program, the National Natural Science Foundation of China (NSFC) (Grant No. 11021262), and from MOST 973 of China (Nr. 2012BC937500). Computation is mainly supported by the Supercomputing Center of CAS.

References

An, J., Voelkl, E., Suk, J.W., Li, X., Magnuson, C.W., Fu, L., Tiemeijer, P., Bischoff, M., Freitag, B., Popova, E., 2011. Domain (grain) boundaries and evidence of " twinlike" structures in chemically vapor deposited grown graphene. ACS nano 5, 2433–2439.

Ariza, M., Ortiz, M., Serrano, R., 2010. Long-term dynamic stability of discrete dislocations in graphene at finite temperature. Int. J. Frac. 166, 215-223.

Ariza, M.P., and Ortiz, M., 2010. Discrete dislocations in graphene. J. Mech. Phys. Solids 58, 710-734.

Blöchl, P.E., 1994. Projector augmented-wave method. Phys. Rev. B 50, 17953-17979.

Castro Neto, A.H., Guinea, F., Peres, N.M.R., Novoselov, K.S., Geim, A.K., 2009. The electronic properties of graphene. Rev. Mod. Phys. 81, 109-162.

Compton, O.C., Cranford, S., Putz, K., An, Z., Brinson, L.C., Buehler, M.J., Nguyen, S.T., 2012. Tuning the Mechanical Properties of Graphene Oxide Paper and Its Associated Polymer Nanocomposites by Controlling Cooperative Intersheet HydrogenBonding. ACS Nano 6, 2008–2019.

Cockayne, E., Rutter, G.M., Guisinger, N.P., Crain, J.N., First, P.N., Stroscio, J.A., 2011. Grain boundary loops in graphene. Phys. Rev. B 83, 195425.

Cranford, S., Buehler, M., 2011. Packing efficiency and accessible surface area of crumpled graphene. Phys. Rev. B 84, 205451.

Devincre, B., Hoc, T., Kubin, L., 2008. Dislocation mean free paths and strain hardening of crystals. Science 320, 1745-1748.

Eshelby, J.D., 1966. A simple derivation of the elastic field of an edge dislocation. Br. J. Appl. Phys. 17, 1131.

Geim, A.K., 2009. Graphene: Status and prospects. Science 324, 1530-1534.

Geim, A.K., Novoselov, K.S., 2007. The rise of graphene. Nat. Mater. 6, 183-191.

Ghosh, S., Calizo, I., Teweldebrhan, D., Pokatilov, E., Nika, D., Balandin, A., Bao, W., Miao, F., Lau, C.N., 2008. Extremely high thermal conductivity of graphene: Prospects for thermal management applications in nanoelectronic circuits. Appl. Phys. Lett. 92, 151911.

Gleiter, H., 1989. Nanocrystalline materials. Prog. Mater. Sci. 33, 223-315.

Grantab, R., Shenoy, V.B., Ruoff, R.S., 2010. Anomalous strength characteristics of tilt grain boundaries in graphene. Science 330, 946-948.

Hall, E.O., 1951. The deformation and ageing of mild Steel: III Discussion of results.

Proc. Phys. Soc. Sec. B 64, 747.

Hashimoto, A., Suenaga, K., Gloter, A., Urita, K., Iijima, S., 2004. Direct evidence for atomic defects in graphene layers. Nature 430, 870-873.

Huang, P.Y., Ruiz-Vargas, C.S., van der Zande, A.M., Whitney, W.S., Levendorf, M.P., Kevek, J.W., Garg, S., Alden, J.S., Hustedt, C.J., Zhu, Y., Park, J., McEuen, P.L., Muller, D.A., 2011. Grains and grain boundaries in single-layer graphene atomic patchwork quilts. Nature 469, 389-392.

Huang, W. Mura, T., 1970. Elastic fields and energies of a circular edge disclination and a straight screw disclination. J. Appl. Phys. 41, 5175.

Hull, D., Bacon, D.J., 2011. Dislocation Arrays and Crystal Boundaries, in: Introduction to Dislocations (Fifth Edition). Butterworth-Heinemann, Oxford, pp. 171-204.

Jeong, B.W., Ihm, J., Lee, G.-D., 2008. Stability of dislocation defect with two pentagon-heptagon pairs in graphene. Phys. Rev. B 78, 165403.

Khare, R., Mielke, S.L., Paci, J.T., Zhang, S., Ballarini, R., Schatz, G.C., Belytschko, T., 2007. Coupled quantum mechanical/molecular mechanical modeling of the fracture of defective carbon nanotubes and graphene sheets. Phys. Rev. B 75, 075412.

Kim, K., Lee, Z., Regan, W., Kisielowski, C., Crommie, M.F., Zettl, A., 2011. Grain boundary mapping in polycrystalline graphene. ACS Nano 5, 2142-2146.

Kim, K.S., Zhao, Y., Jang, H., Lee, S.Y., Kim, J.M., Kim, K.S., Ahn, J.-H., Kim, P., Choi, J.-Y., Hong, B.H., 2009. Large-scale pattern growth of graphene films for stretchable transparent electrodes. Nature 457, 706-710.

Kim, R.H., Bae, M.H., Kim, D.G., Cheng, H., Kim, B.H., Kim, D.H., Li, M., Wu, J., Du, F., Kim, H.S., Kim, S., Estrada, D., Hong, S.W., Huang, Y., Pop, E., Rogers, J.A., 2011. Stretchable, transparent graphene interconnects for arrays of microscale inorganic light emitting diodes on rubber substrates, Nano Lett. 11, 3881-3886.

Kleman, M., Friedel, J., 2008. Disclinations, dislocations, and continuous defects: A reappraisal. Rev. Mod. Phys. 80, 61-115.

Koenig, S.P., Boddeti, N.G., Dunn, M.L., Bunch, J.S., 2011. Ultrastrong adhesion of graphene membranes. Nat. Nano 6, 543-546.

Koh, Y.K., Bae, M.-H., Cahill, D.G., Pop, E., 2010. Heat conduction across monolayer and few-layer graphenes. Nano Lett. 10, 4363-4368.

Kolesnikova, A.L., Romanov, A.E., 1998. A disclination-based approach to describing the structure of fullerenes. Phys. Solid State 40, 1075-1077.

Kresse, G., Furthmüller, J., 1996a. Efficiency of ab-initio total energy calculations for metals and semiconductors using a plane-wave basis set. Comput. Mat. Sci. 6, 15-50.

Kresse, G., Furthmüller, J., 1996b. Efficient iterative schemes for ab initio total-energy calculations using a plane-wave basis set. Phys. Rev. B 54, 11169-11186.

Kresse, G., Joubert, D., 1999. From ultrasoft pseudopotentials to the projector augmented-wave method. Phys. Rev. B 59, 1758-1775.

Kurasch, S., Kotakoski, J., Lehtinen, O., Skakalova, V., Smet, J., Krill, C.E., 3rd, Krasheninnikov, A.V., Kaiser, U., 2012. Atom-by-atom observation of grain boundary migration in graphene. Nano Lett 12, 3168-3173.

Lee, C., Wei, X., Kysar, J.W., Hone, J., 2008. Measurement of the elastic properties and intrinsic strength of monolayer graphene. Science 321, 385-388.

Li, J.C.M., 1972. Disclination model of high angle grain boundaries. Surf. Sci. 31, 12-26.

Li, X., Cai, W., An, J., Kim, S., Nah, J., Yang, D., Piner, R., Velamakanni, A., Jung, I., Tutuc, E., Banerjee, S.K., Colombo, L., Ruoff, R.S., 2009. Large-area synthesis of high-quality and uniform graphene films on copper foils. Science 324, 1312-1314.

Lin, Y.-M., Dimitrakopoulos, C., Jenkins, K.A., Farmer, D.B., Chiu, H.-Y., Grill, A., Avouris, P., 2010. 100-GHz transistors from wafer-scale epitaxial graphene. Science 327, 662.

Liu, F., Ming, P., Li, J., 2007. Ab initio calculation of ideal strength and phonon instability of graphene under tension. Phys. Rev. B 76, 064120.

Liu, Y., Xu, Z., Zheng, Q., 2011. The interlayer shear effect on graphene multilayer

resonators. J. Mech. Phys. Solids 59, 1613-1622.

Müllner, P., Pirouz, P., 1997. A disclination model for the twin-twin intersection and the formation of diamond-hexagonal silicon and germanium. Mater. Sci. Eng. A 233, 139-144.

Malola, S., Häkkinen, H., Koskinen, P., 2010. Structural, chemical, and dynamical trends in graphene grain boundaries. Phys. Rev. B 81, 165447.

Meyer, J.C., Girit, C.O., Crommie, M.F., Zettl, A., 2008. Imaging and dynamics of light atoms and molecules on graphene. Nature 454, 319-322.

Monkhorst, H.J., Pack, J.D., 1976. Special points for Brillouin-zone integrations. Phys. Rev. B 13, 5188-5192.

Muskhelishvili, N.I., 1953. Some basic problems of the mathematical theory of elasticity. 3rd ed, p94, p229 (P. Noordhoff Ltd.,Groningen-Holland).

Nix, W.D., Gao, H., 1998. Indentation size effects in crystalline materials: A law for strain gradient plasticity. J. Mech. Phys. Solids 46, 411-425.

Perdew, J.P., Burke, K., Ernzerhof, M., 1996. Generalized gradient approximation made simple. Phys. Rev. Lett. 77, 3865-3868.

Perdew, J.P., Burke, K., Ernzerhof, M., 1997. Generalized gradient approximation made simple. Phys. Rev. Lett. 78, 1396-1396.

Pereira, V.M., Castro Neto, A.H., Peres, N.M.R., 2009. Tight-binding approach to uniaxial strain in graphene. Phys. Rev. B 80, 045401.

Petch, N.J., 1953. The cleavage strength of polystrals. J. Iron Steel Inst. 174, 25–28.

Plimpton, S., 1995. Fast parallel algorithms for short-range molecular dynamics. J. Comput. Phys. 117, 1-19. http://lammps.sandia.gov.

Rasool, H.I., Song, E.B., Allen, M.J., Wassei, J.K., Kaner, R.B., Wang, K.L., Weiller, B.H., Gimzewski, J.K., 2010. Continuity of graphene on polycrystalline copper. Nano Lett. 11, 251-256.

Reina, A., Jia, X., Ho, J., Nezich, D., Son, H., Bulovic, V., Dresselhaus, M.S., Kong, J., 2008. Large Area, few-layer graphene films on arbitrary substrates by chemical vapor deposition. Nano Lett. 9, 30-35.

Rogers, J.A., Lagally, M.G., Nuzzo, R.G., 2011. Synthesis, assembly and applications

of semiconductor nanomembranes. Nature 477, 45-53.

Romanov, A.E., Kolesnikova, A.L., 2009. Application of disclination concept to solid structures. Prog. Mater. Sci. 54, 740-769.

Sen, D., Novoselov, K.S., Reis, P.M., Buehler, M.J., 2010. Tearing graphene sheets from adhesive substrates produces tapered nanoribbons. Small 6, 1108-1116.

Seol, J.H., Jo, I., Moore, A.L., Lindsay, L., Aitken, Z.H., Pettes, M.T., Li, X., Yao, Z., Huang, R., Broido, D., Mingo, N., Ruoff, R.S., Shi, L., 2010. Two-dimensional phonon transport in supported graphene. Science 328, 213-216.

Shih, K.K., Li, J.C.M., 1975. Energy of grain boundaries between cusp misorientations. Surf. Sci. 50, 109-124.

Stuart, S.J., Tutein, A.B., Harrison, J.A., 2000. A reactive potential for hydrocarbons with intermolecular interactions. J. Chem. Phys. 112, 6472-6486.

Taylor, G.I., 1934. The mechanism of plastic deformation of crystals. Part I. Theoretical. Proceedings of the Royal Society of London. Series A 145, 362-387.

Wang, B., Puzyrev, Y., Pantelides, S.T., 2011. Strain enhanced defect reactivity at grain boundaries in polycrystalline graphene. Carbon 49, 3983-3988.

Warner, J.H., Margine, E.R., Mukai, M., Robertson, A.W., Giustino, F., Kirkland, A.I., 2012. Dislocation-driven deformations in graphene. Science 337, 209-212.

Wei, Y., Wu, J., Yin, H., Shi, X., Yang, R., Dresselhaus, M., 2012. The nature of strength enhancement and weakening by pentagon-heptagon defects in graphene. Nat. Mater. 11, 759-763.

Wei, Y., Wang, B., Wu, J., Yang, R., Dunn, M.L., 2012. Bending rigidity and Gaussian bending stiffness of single-layered graphene. Nano Lett. doi: 10.1021/nl303168w.

Wu, J., Shi, X., Wei, Y., 2012. Tunable band structures of polycrystalline graphene by external and mismatch strains. Acta Mech. Sinica, DOI 10.1007/s10409-012-0164-x.

Yazyev, O.V., Louie, S.G., 2010a. Electronic transport in polycrystalline graphene. Nat. Mater. 9, 806-809.

Yazyev, O.V., Louie, S.G., 2010b. Topological defects in graphene: Dislocations and grain boundaries. Phys. Rev. B 81, 195420.

Yu, H.Y., Sanday, S.C., 1991. Disclinations in bimaterials. Phys. Status Solidi (a) 126, 355-365.

Yu, Q., Jauregui, L.A., Wu, W., Colby, R., Tian, J., Su, Z., Cao, H., Liu, Z., Pandey, D., Wei, D., Chung, T.F., Peng, P., Guisinger, N.P., Stach, E.A., Bao, J., Pei, S.-S., Chen, Y.P., 2011. Control and characterization of individual grains and grain boundaries in graphene grown by chemical vapour deposition. Nat. Mater. 10, 443-449.

Zhang, T., Li, X., Kadkhodaei, S., Gao, H., (2012). Flaw insensitive fracture in nanocrystalline graphene Nano Letters 12, 4605-4610.

Zhang, X., Jiao, K., Sharma, P., Yakobson, B., 2006. An atomistic and non-classical continuum field theoretic perspective of elastic interactions between defects (force dipoles) of various symmetries and application to graphene. J. Mech. Phys. Solids 54, 2304-2329.

Zhao, X., Zhang, Q., Chen, D., Lu, P., 2010. Enhanced mechanical properties of graphene-based poly(vinyl alcohol) composites. macromolecules 43, 2357-2363.

Zhou, J., Huang, R., 2008. Internal lattice relaxation of single-layer graphene under in-plane deformation. J. Mech. Phys. Solids 56, 1609-1623.